Volume 26
Number 23
21 June 2024
Pages 16391–16912

PCCP

Physical Chemistry Chemical Physics

rsc.li/pccp

25 YEARS ANNIVERSARY

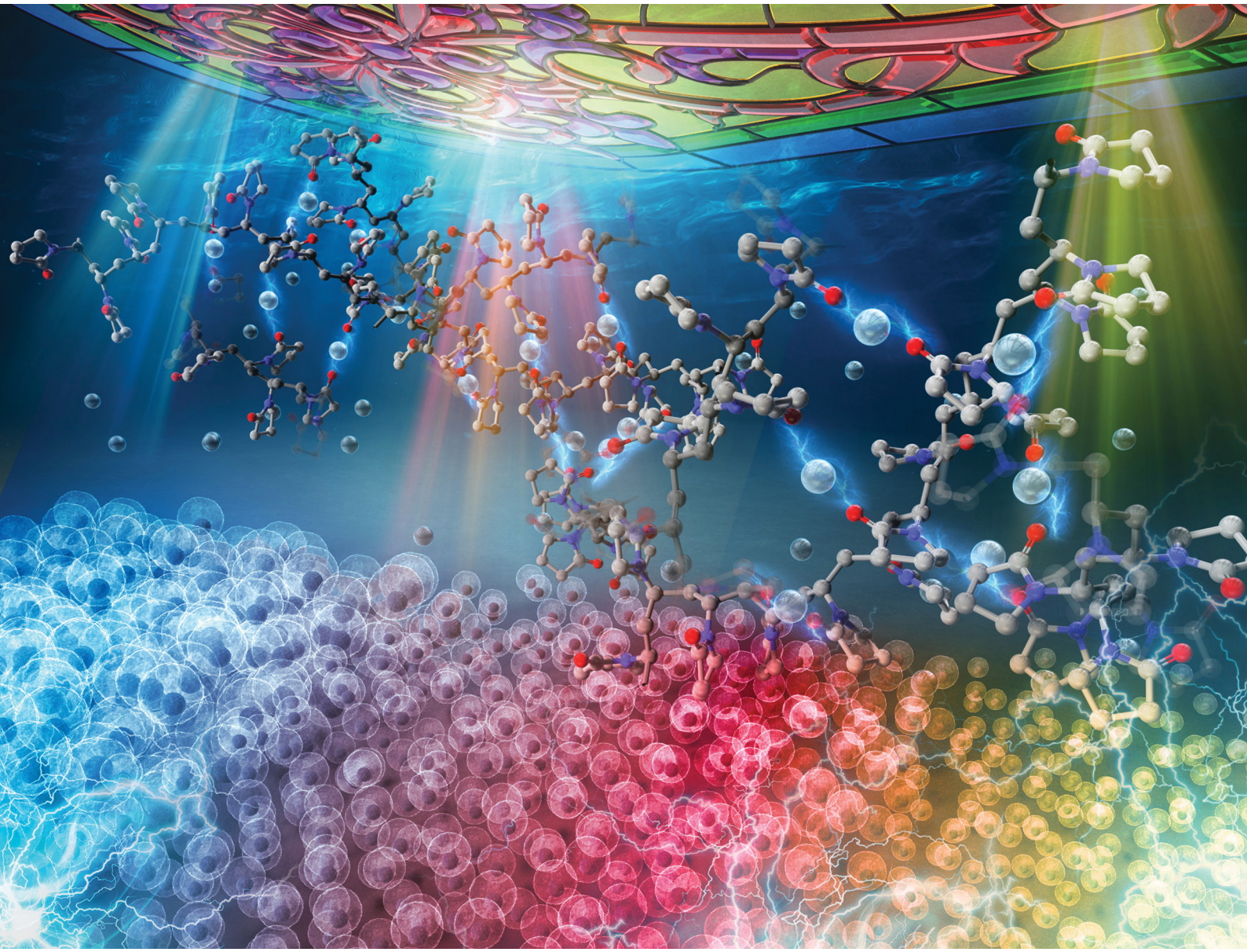

ISSN 1463-9076

ROYAL SOCIETY OF CHEMISTRY

PAPER

Norihisa Kobayashi *et al.*

The effect of a polymer capping agent on electrodeposited silver nanoparticles in a silver deposition-based electrochromic device

PCCP Owner Societies

PCCP

ROYAL SOCIETY OF CHEMISTRY

PAPER

View Article Online
View Journal | View Issue

Cite this: *Phys. Chem. Chem. Phys.*, 2024, **26**, 16466

The effect of a polymer capping agent on electrodeposited silver nanoparticles in a silver deposition-based electrochromic device†

Shun Uji, Kazuki Nakamura and Norihisa Kobayashi *

Received 26th December 2023,
Accepted 21st March 2024

DOI: 10.1039/d3cp06281c

rsc.li/pccp

In this study, polyvinylpyrrolidone (PVP) was introduced into an Ag deposition-based electrochromic (EC) device as a capping agent for electrodeposited Ag nanoparticles (AgNPs) to improve the coloration characteristics of EC devices and to precisely control the size and shape of the AgNPs. Through the coordination of PVP molecules with Ag^+ ions in the EC electrolyte, the critical voltage for the deposition of AgNPs decreased, resulting in a lower operating voltage of the EC device in comparison with the conventional one. Because particle growth and AgNP aggregation were suppressed by the capping effect of PVP, uniform electrodeposition of AgNPs was achieved. Aggregation suppression enabled vivid cyan, yellow, and red coloration using a simple driving procedure. The suppression of AgNP aggregation by PVP was demonstrated even in an electrochemical system. Furthermore, the capping effect of PVP also improved image retention. Better color retention properties were achieved even without the use of any counter-modified electrode cells.

1. Introduction

The electrochromic (EC) phenomenon involves reversible optical changes resulting from EC materials undergoing electrochemical redox reactions.[1–4] The color change of an EC device is based on a change in the electronic state of an EC material caused by the electron transfer between the EC material and the electrode.

Several studies on EC materials, including organic and inorganic compounds, have been published.[5–12] Devices using EC materials offer many advantages over self-emission displays, including low operating voltages, color retention, and high visibility under sunlight.[13–15] Therefore, EC materials are expected to be applied in information displays (*e.g.*, electronic paper and digital signage) and light-modulating devices (*e.g.*, light shutters, smart windows, and variable reflectance mirrors).[16–22] Among these, inorganic EC materials have attracted significant interest owing to their electrochemical stability and practical applications. Inorganic EC materials can be classified into two types. The first group comprises transition metal oxides such as WO_3, NiO, and MoO_3.[23–28] When the valence of the metal oxide films is changed by an applied voltage, a cation with a small ionic radius (H^+, Li^+, *etc.*) is inserted into the crystal lattice of the metal oxide owing to charge compensation, resulting in a change in coloration. The second group of EC materials comprises metals that can undergo reversible electrodeposition, such as Ag, Bi, Cu, and Ni.[29–37] In such systems, the achromatic colors, such as metallic mirrors, black and white, are elicited owing to the electrodeposition of reduced metal cations on a transparent conductive electrode. To develop a full-color EC device, it is desirable to achieve stable multicolor representation in a single pixel with a simple structure. For this purpose, unlike organic EC materials, inorganic EC materials have some disadvantages with regard to multi-coloration due to the difficulties posed by multi-step redox reactions.

To address this issue, we report an EC device based on the deposition and dissolution of silver nanoparticles (AgNPs) that achieves seven optical states: transparent, silver mirror, black, three primary colors (cyan, magenta, and yellow), and green.[33,38–44] The underlying mechanism of such multi-coloration is based on controlling the morphology of the electrodeposited AgNPs on a transparent electrode, such as an indium tin oxide (ITO) electrode. The Ag deposition-based EC device has a very simple structure, consisting only of an Ag^+-containing gel electrolyte sandwiched between a pair of ITO electrodes. The default state of an EC device is transparent, whereas applying a negative voltage to the device causes Ag electrodeposition on the surface of the electrode. It is noteworthy that this EC device can change color based on the simple electrochemical deposition and dissolution of Ag, thus achieving an EC device with sufficient stability over thousands of cycles.[33,45]

Graduate School of Engineering, Chiba University, 1-33, Yayoi-cho, Inage-ku, Chiba, 263-8522, Japan. E-mail: koban@faculty.chiba-u.jp; Fax: +81-43-290-3457; Tel: +81-43-290-3458

† Electronic supplementary information (ESI) available. See DOI: https://doi.org/10.1039/d3cp06281c

Chromatic colors such as cyan, magenta, yellow, and green occur due to light absorption by localized surface plasmon resonance (LSPR) of the electrodeposited AgNPs. The wavelength of the LSPR band is known to shift depending on the size and shape of the metal nanoparticles.[46–48] Therefore, drastic color changes can be achieved by manipulating the LSPR bands based on the morphology of the AgNPs. For this purpose, the ''voltage-step method'' is applied to the Ag deposition-based EC device to obtain chromatic colors through morphology control of the electrodeposited AgNPs.[49–51] Two voltages are applied in this method (Fig. S1, ESI†); the first voltage V_1 is applied for a very short time (t_1) to initiate Ag nucleation; subsequently, the second voltage V_2 is applied for an arbitrary time (t_2) to promote Ag nuclei growth. As V_2 is more positive than the nucleation voltage, further nucleation is no longer possible at t_2. Therefore, the resultant device color, which is attributed to the size and density of the AgNPs, can be controlled by varying the voltage-step parameters (V_1, t_1, V_2, and t_2).

Using the voltage-step method, cyan and magenta colors of the Ag deposition-based EC device were obtained through the formation of aggregated anisotropic AgNPs.[38,43] The coalescence of the AgNPs caused the broadening of the LSPR band, which resulted in a dark color, indicating low purity. As mentioned previously, the wavelength and width of the LSPR bands depend on the morphology of the electrodeposited AgNPs. For further color variation and improvement in the color purity of the Ag deposition-based EC devices, it is essential to obtain coloration from isolated AgNPs whose size and shape are precisely controlled in the absence of aggregation.

In the case of the chemical reaction-based synthesis of AgNPs, various approaches for producing AgNPs with anisotropic shapes have been implemented using several techniques, such as additives, lasers, photoirradiation, and sonication.[52–63] However, there have been few reports on controlling the morphology of electrochemically deposited AgNPs. Only spherical AgNPs or their coalescent structures were generated in a previously reported Ag deposition-based EC device using the voltage-step method. Although the most common method for controlling the morphology of AgNPs is to introduce a capping agent for the metal particles, the electrochemical instability of the capping agent limits its application in EC devices.

In this study, we aimed to prevent the strong aggregation of electrodeposited AgNPs by employing polyvinylpyrrolidone (PVP) as the capping agent in an Ag deposition-based EC device. The chemical synthesis of AgNPs generally uses PVP as a capping agent because of its capacity to disperse metal nanoparticles in solutions.[64–66] If PVP prevents AgNP aggregation, even during electrochemical deposition, the introduction of capping agents is expected to be a novel method for controlling the morphology of electrodeposited AgNPs. In this study, the effects of introducing PVP in an Ag deposition-based EC device on the electrochemical properties and morphology of the AgNPs, as well as the optical properties of the EC device, were investigated in detail.

2. Experimental section

2.1. Materials

Silver(I) nitrate ($AgNO_3$, FUJIFILM Wako Pure Chemical Corporation, Japan), copper(II) chloride ($CuCl_2$, Kanto Chemical Co., Inc., Japan), lithium bromide (LiBr, Kanto Chemical Co., Inc., Japan), dimethyl sulfoxide (DMSO, Sigma Aldrich, Japan), polyvinylpyrrolidone (PVP, K30, $M_w = 4.0 \times 10^4$, TCI Chemicals, Japan), and polyvinyl butyral (PVB, B60T, $M_w = 5.5 \times 10^4$, Kuraray Co. Ltd, Japan) were used as received. ITO-coated glass substrates 720 μm thick (4.2 Ω $\square^{-1}$) were used after washing and ozonation.

2.2. Preparation of the EC electrolyte

Several electrolytes for the three-electrode EC cell and the two-electrode EC device were prepared to confirm the effect of the PVP capping agent. 10 mM $AgNO_3$ as the EC material, 10 mM $CuCl_2$ as the counter-reaction material and electrochemical mediator, and 50 mM LiBr as the supporting electrolyte were dissolved in DMSO. Subsequently, 10 mM PVP, acting as a capping and gelling agent, or 2.4 mM PVB, acting as a gelling agent (the conventional electrolyte in Ag deposition-based EC devices), was mixed into the DMSO-based electrolyte solution to prepare the gel electrolyte. For comparison, a DMSO-based EC electrolyte without any gelling agents and an electrolyte containing only PVP and LiBr were also prepared.

2.3. Fabrication of the EC device

A three-electrode Ag deposition-based EC cell was prepared using an ITO electrode as the working electrode, Pt wire as the counter electrode, and Ag/Ag^+ as the reference electrode. The EC devices were fabricated by placing three types of electrodes and electrolytes into a 1 cm × 1 cm optical cell. A two-electrode Ag deposition-based EC device was fabricated by sandwiching a gel electrolyte between two ITO electrodes. The effective electrode area of this EC device was set to 1 cm × 1 cm, and the distance between the electrodes was maintained at 300 μm using a spacer. In this study, the EC devices with the PVP- or PVB-based electrolytes were labeled ''P-ECD'' and ''B-ECD'', respectively.

2.4. Apparatus

A potentiostat/galvanostat (ALS/CHI 660A, ALS Co., Ltd, Japan) was used to apply a voltage to the EC device. The reference electrode was prepared by injecting an Ag^+ solution (10 mM $AgNO_3$ and 100 mM TBAP in acetonitrile) into a sample holder with ion-permeable glass (BAS, Japan) and then sealing the holder with a cap containing an Ag wire. The transmittance and absorption spectra were recorded using a diode array detection system (USB4000, Ocean Insight, Japan) and a tungsten halogen lamp (HL-2000-LL, Ocean Insight, Japan) as the light source. The transmittance and absorption spectra of the EC device before the voltage application were used as references. The electrode potentials of the working/reference or counter/reference electrodes were recorded using two potentiostats (ALS/CHI 660A, ALS Co., Ltd, Japan and HAG1232m, HOKUTO

DENKO, Japan). The morphology of the AgNPs electrodeposited on the working electrode was observed using field-emission scanning electron microscopy (FE-SEM; JSM-6510, JEOL, Japan). An X-ray photoelectron spectrometer (JPS-9030, JEOL, Japan) was used for the XPS measurements. The viscosity of the electrolytes was measured with a viscometer (VISCO-895, ATAGO, Japan).

3. Results and discussion

First, the effect of PVP on the electrochemical properties of the Ag deposition-based EC device was studied. The cyclic voltammetry results and changes in the transmittance at 500 nm for the three-electrode EC cell are shown in Fig. 1. Cyclic voltammograms of the DMSO-based electrolyte containing only LiBr and PVP are shown in Fig. 1 (blue line). Electric current derived from the electrochemical reaction of the materials was not observed, and PVP was not reactive in the potential sweep range for Ag deposition and dissolution. In the conventional EC electrolyte without PVP (Fig. 1, black line), after reaching the reduction peak of Cu^{2+} ion at −0.7 V when the potential was scanned from 0 V in the negative direction, an apparent cathodic current from Ag^+ reduction was observed at −1.28 V (*vs.* Ag/Ag^+). When a potential more negative than −1.28 V was applied, the cell transmittance decreased as a result of Ag electrodeposition on the electrode; this result indicated that the critical potential for Ag deposition was −1.28 V. In the case of the EC electrolyte containing PVP (Fig. 1, red line), Ag^+ ions began to be reduced after the reduction of Cu^{2+} ions; the critical potential for Ag deposition was −1.15 V, which is 0.13 V lower than that of the electrolyte without PVP. In our previous study, we showed that when Ag^+ and Br^- ions are present in an electrolyte, they form $AgBr_n^{(1-n)}$ complex species.[67] In contrast, it has been reported that PVP molecules form complexes with Ag^+ ions through coordination.[68,69] Hence, the difference between the critical voltages with and without PVP can be attributed to a change in the complex structure. To confirm whether Br^- or PVP preferentially formed a complex structure with Ag^+, PVP was added to an electrolyte containing 50 mM of Br^- coordinated to 10 mM of Ag^+ ions (forming the $AgBr_n^{(1-n)}$ complexes species, as mentioned above); the equilibrium electrode potential for the Ag/Ag^+ redox reaction in the electrolyte solution was then measured. An AgS wire, acting as an indicating electrode, and the Ag/Ag^+ reference electrode were put into the EC electrolyte containing the Br^- and Ag^+ complex species (similar to Fig. 1, black line) to measure the spontaneous potential change when PVP was gradually added (Fig. S2, ESI†). Although the electrode potential of the $AgBr_n^{(1-n)}$-containing electrolyte was −0.64 V (*vs.* Ag/Ag^+) before adding PVP, the electrode potential increased to −0.58 V after adding PVP. This result indicates that adding PVP promoted the formation of another type of complex, that between PVP and Ag^+ ions, instead of $AgBr_n^{(1-n)}$. This change in the equilibrium potential affects the reduction potential of the electrolytes, as shown in Fig. 1.

Subsequently, two-electrode devices were fabricated using two types of electrolytes. The first device is a DMSO-based electrolyte containing Ag^+ ions and PVB in a DMSO-based electrolyte (B-ECD). This electrolyte has been reported previously, and PVB is thought to act as only a gelling agent without a capping effect on the deposited AgNPs. The other electrolyte contained PVP in the DMSO-based electrolyte (P-ECD). The cyclic voltammograms and changes in the transmittance at 500 nm for the two EC devices according to the voltage sweep are shown in Fig. 2. From the cyclic voltammograms and corresponding transmittance changes, AgNPs were found to be deposited on the surface of the working electrode in both EC devices. However, the critical voltages for Ag deposition were completely different; the critical voltage of the P-ECD was −1.20 V, whereas that of B-ECD was −2.02 V. The critical voltage for Ag deposition was shifted by 0.82 V in the positive direction by the addition of PVP. This difference in the critical voltage for Ag deposition (0.82 V) is significantly larger than that in the critical potential (0.13 V *vs.* Ag/Ag^+) obtained in the three-electrode EC cell. Therefore, this difference cannot be explained only by the formation of PVP with Ag^+.

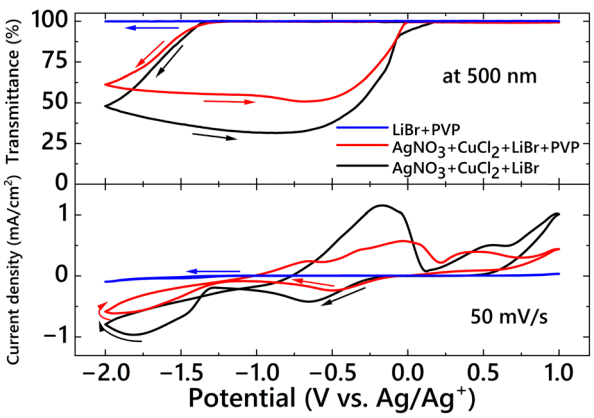

Fig. 1 Change in transmittance at 500 nm (top) and cyclic voltammogram (bottom) of the three-electrode EC cell with various EC electrolytes (blue: LiBr and PVP in DMSO; red: $AgNO_3$, $CuCl_2$, LiBr, and PVP in DMSO; black: $AgNO_3$, $CuCl_2$, and LiBr in DMSO).

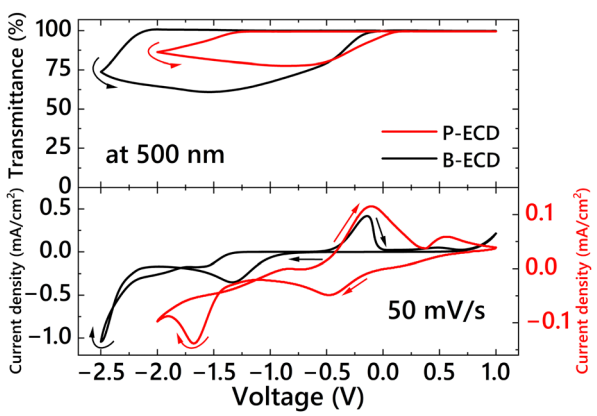

Fig. 2 Change in the transmittance at 500 nm (top) and cyclic voltammograms (bottom) of the two-electrode EC devices: P-ECD (red) and B-ECD (black).

To monitor the changes in the potentials of the cathode (working electrode) and anode (counter electrode) during voltage sweeping, a system for electrode potential measurements was fabricated, as shown in Fig. S3 (ESI†).[70] Two ITO electrodes and an Ag/Ag^+ reference electrode were placed in a 1 cm × 1 cm optical cell filled with PVP- or PVB-based electrolytes. The same electrolytes were used as those in the two-electrode EC devices (P-ECD and B-ECD). Two potentiostats were used for this measurement: the first potentiostat was connected between two ITO electrodes to apply the operating voltage, and the second was connected between the reference electrode and the cathode or anode to measure the electrode potentials. The changes in electrode potentials during the voltage sweeps and two-electrode voltammograms are shown in Fig. 3. For the PVB-based electrolyte (Fig. 3, black), the electrode potential in the initial state (short-circuit conditions) was almost 0 V (*vs.* Ag/Ag^+). After starting the voltage sweep from 0 V, the cathode potential did not change in the voltage range of 0 V to −0.7 V, whereas the anode potential increased. The cathode potential started to shift negatively when a −0.7 V voltage was applied, and the cathode potential reached −1.28 V (*vs.* Ag/Ag^+), coinciding with the critical potential for Ag deposition when a −2.02 V voltage was applied between the anode and cathode. On the other hand, when PVP was introduced into the electrolyte (Fig. 3, red), the potential of both electrodes in the initial state (short-circuit condition) was −0.12 V (*vs.* Ag/Ag^+). This difference in the electrode potentials in the initial state between the PVB and PVP electrolytes coincided with the difference in the complexation states of the Ag^+ ions (with Br^- or PVP). After starting the voltage sweep, the cathode potential drastically shifted to a negative value, whereas the anode maintained a potential of approximately 0 V (*vs.* Ag/Ag^+). The cathode potential reached a critical value of −1.15 V (*vs.* Ag/Ag^+) when a voltage of −1.20 V was applied between the anode and cathode. The difference in the changing behavior of the electrode potential between the PVB- and PVP-based electrolytes during voltage sweeping can be attributed to the reactivity of the complex between the PVP and metal ions. In the case of a two-electrode device, the balance of redox reactions at the cathode and anode influences the electrochemical properties of the EC device. If the anodic reaction is more likely to occur rather than the cathodic reaction at a certain voltage, the anode potential is maintained during voltage application. In this case, the cathode potential should be shifted to compensate for charge consumption in the device. Consequently, the cathode potential reached a critical potential for Ag deposition even when a lower voltage was applied. To confirm the reactivity of the anodic material in the PVB- and PVP-based electrolytes, cyclic voltammetry measurements were conducted in the positive direction from 0 V using a three-electrode EC cell (Fig. 4). A definite current was observed from 0 V in the positive direction owing to the oxidation reaction in the PVP-based electrolyte (Fig. 4, red), whereas almost no redox current was observed in the PVB-based electrolyte (Fig. 4 black). This reaction in the PVP electrolyte was due to the oxidation of Cu^+ to Cu^{2+} ions. In the PVP-based electrolyte, Cu^+ ions may be generated by PVP complexation. An appropriate explanation for the generation of Cu^+ in the presence of PVP (possibly by the reaction with PVP) is not currently available. However, the oxidation potential fully coincided with that of Cu^+ oxidation to Cu^{2+}. Thus, the operating voltage of the two-electrode EC device was significantly reduced by introducing PVP into the EC electrolyte.

Next, the effect of PVP on coloration characteristics was investigated by applying coloration voltages to the EC devices. First, a constant voltage of −2.5 V was applied to the P-ECD for 120 s. The change in the absorption spectra of the P-ECD during the voltage application is shown in Fig. 5(a). The absorption spectrum at 30 s showed two LSPR peaks at approximately 480 and 600 nm; subsequently, the LSPR band

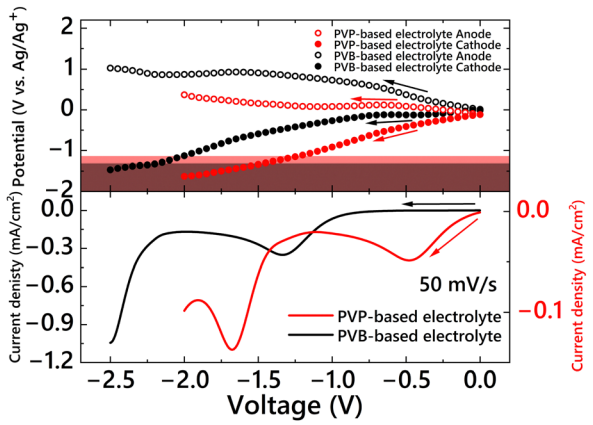

Fig. 3 Changes in the electrode potential of the anodes (white bullets) and cathodes (bullets) during voltage sweep (top) and voltammograms (bottom) of two-electrode EC cells: PVP-based electrolyte (red line) and PVB-based electrolyte (black line). The red and black areas indicate the potential range for AgNP electrodeposition in PVP- and PVB-based electrolytes, respectively (refer to Fig. 1).

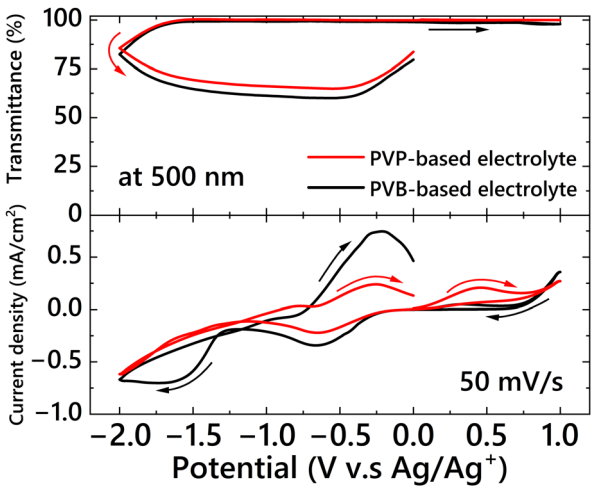

Fig. 4 Change in transmittance at 500 nm (top) and cyclic voltammogram (bottom) of the three-electrode EC cell; PVP-based electrolyte (red line) and PVB-based electrolyte (black line), scanned from 0 V in the positive direction.

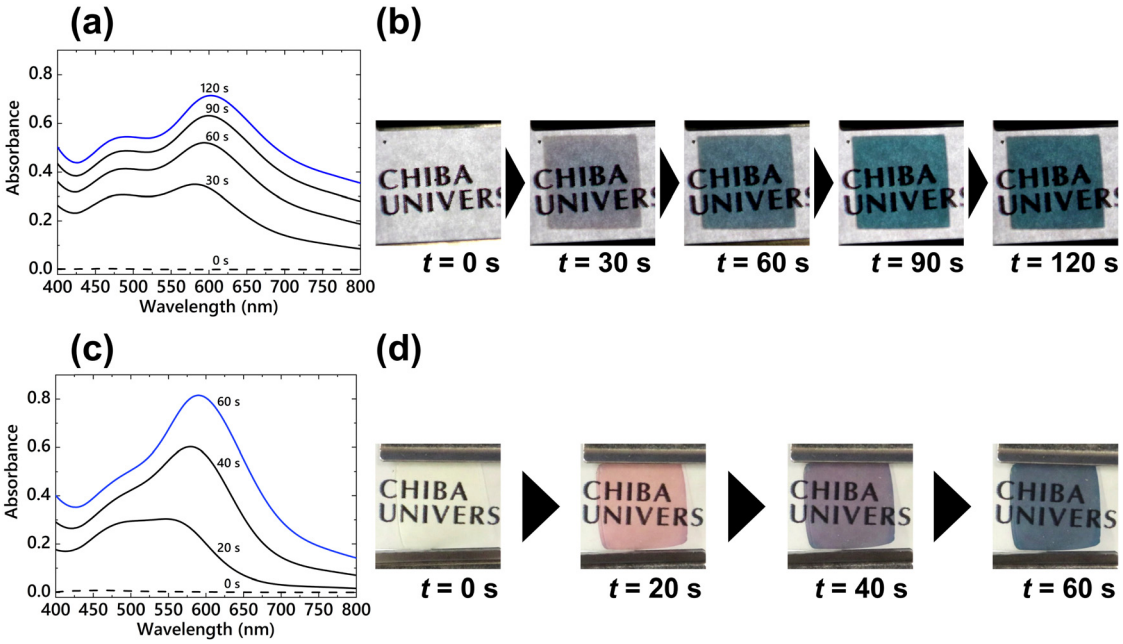

Fig. 5 The change of absorption spectra (a) and device images (b) of the P-ECD during constant voltage application (V = −2.5 V, t = 120 s). The change of absorption spectra (c) and device images (d) of the B-ECD during step voltage application (V_1 = −3.5 V, t_1 = 100 ms, V_2 = −1.6 V, t_2 = 60 s).

at approximately 600 nm increased in priority with continuous voltage application. As a result, the P-ECD successfully elicited cyan color by applying a constant voltage for 120 s (Fig. 5(b)). In our study, using B-ECD, a thicker Ag layer was formed, and the EC device represented a mirror state by applying the same constant voltage of −2.5 V (Fig. S4, ESI†) because both the nucleation reaction and subsequent growth of nuclei occur in succession with voltage application.[33,38] However, this P-ECD achieved vivid cyan coloration despite the application of a constant voltage with a sufficient overvoltage. Also, the cyan coloration of the P-ECD returned to its original transparent state by applying an oxidation voltage of +0.7 V for 20 s. To compare with the P-ECD, cyan coloration was achieved by applying a step voltage (V_1 = −3.5 V, t_1 = 100 ms and V_2 = −1.6 V, t_2 = 60 s) to the B-ECD (Fig. 5(c) and (d)). The absorption peaks appeared at 20 s after the voltage was applied at approximately 490 and 550 nm; the B-ECD elicited a magenta-like color (Fig. 5(d)). Subsequently, the absorption peak with a longer wavelength shifted to 590 nm by applying V_2, and the device exhibited a cyan color at 60 s after starting the voltage application. In addition, an oxidation voltage of +0.5 V for 20 s could bleach this cyan-colored B-ECD. There is an apparent difference in the driving voltage and change in the absorption spectra for obtaining the cyan coloration between the P-ECD and B-ECD. In the P-ECD, the absorption spectra displayed two distinct peaks, and the absorbance on the longer wavelength band increased with a slight red shift of the LSPR band at approximately 5 nm. For the B-ECD, the absorption peak at the long-wavelength side was redshifted by approximately 40 nm by the application of a growth voltage. This difference could be due to the change in the state of the electrodeposited AgNPs owing to the addition of different polymers.

The morphologies of the deposited AgNPs were observed using FE-SEM to study their structures in detail. The FE-SEM images of the electrode surface of the P-ECD with constant voltage application for cyan coloration (V = −2.5 V, t = 120 s) are shown in Fig. 6(a). The diameter of the single electrodeposited AgNPs was approximately 35 nm; the AgNPs in the P-ECD were densely electrodeposited without coalescence despite the application of a constant voltage. In the cross-sectional image of the electrode (Fig. 6(b)), three layers were observed: the glass substrate, an ITO layer, and an AgNP layer. The thickness of the AgNP layer was ~50 nm, and a relatively flat surface was formed. An FE-SEM image of the electrode surface of the B-ECD with cyan coloration obtained by applying a step voltage is shown in Fig. 6(c); the electrodeposited AgNPs formed large aggregates. In the cross-sectional image of the cyan-colored B-ECD electrode (Fig. 6(d)), the AgNPs formed a rough surface due to the large clumps. These results indicate that PVP appeared to act as a capping agent for the AgNPs and prevented the particles from aggregating, resulting in the formation of a flat Ag layer in comparison with B-ECD. In addition, because PVP suppressed AgNP growth, the Ag layer became thinner, and a cyan color was elicited even when a constant voltage was applied, which usually represents a mirror-like optical state.[33,38] This result can also be supported by the amount of Ag reduction charges shown in Fig. 1, bottom. Plasmon coupling occurs and induces the appearance of a new LSPR band when plasmonic particles, such as AgNPs, approach each other.[71,72] The LSPR band due to the plasmon coupling was induced in a longer wavelength region than that of the single nanoparticles. Moreover, as the plasmon coupling between the particles becomes stronger or the particles become irregularly shaped, the LSPR band shifts to longer wavelengths.[43] In the

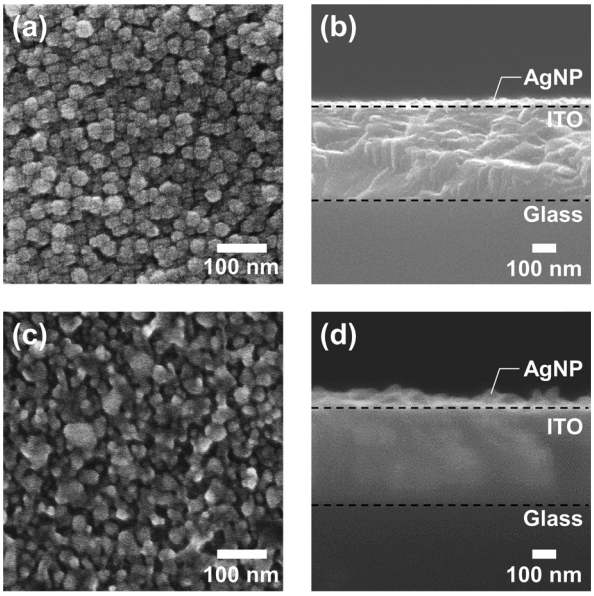

Fig. 6 FE-SEM images of the surface (a) and cross-section (b) of the P-ECD electrode where AgNPs were electrodeposited after a constant voltage application (V = −2.5 V, t = 120 s). FE-SEM images of the surface (c) and cross-section (d) of the B-ECD electrode where AgNPs were electrodeposited after a step voltage application (V_1 = −3.5 V, t_1 = 100 ms, V_2 = −1.6 V, t_2 = 60 s).

B-ECD, particle nuclei were generated uniformly on the electrode by nucleation voltage and grew by the application of the growth voltage. By increasing the AgNP growth, the number of couplings and aggregations of the growing AgNPs gradually increased, resulting in the formation of complicated deposited structures, as shown in Fig. 6(c). This large change in the morphology of the deposited AgNPs caused a redshift in the absorption peak and induced a color change from magenta to cyan.[38] In contrast, excessive coalescence and coupling of the AgNPs were not observed in the P-ECD, and spherical AgNPs were uniformly deposited due to PVP capping, as shown in Fig. 6(a). Since irregular morphology growth and excessive aggregation, as observed in the B-ECD, were prevented by the capping effect of PVP, the redshift of the LSPR peak was small, resulting in vivid cyan coloration. Therefore, the capping effect of PVP was achieved in the Ag deposition-based EC device, indicating that the morphology of the electrodeposited AgNPs could be controlled by the additive species.

XPS measurements were performed to identify the presence of PVP molecules in the deposited AgNPs. Fig. S5(a) (ESI†) shows the XPS spectra of the electrode of cyan-colored Ag deposits in the P-ECD and B-ECD electrolytes in the range of 0–1000 eV. In the P-ECD, C, N, O, Ag, In, and Sn signals were observed, and the In and Sn signals were ascribed to the ITO electrode. In the B-ECD, C, O, Ag, In, and Sn signals were observed; however, N signals were not observed. A detailed comparison of the Ag 3d and N 1s signals is shown in Fig. S5(b) and (c) (ESI†), respectively. The $3d_{3/2}$ and $3d_{5/2}$ Ag signals were observed at the same binding energies in the P-ECD and B-ECD films. Since the amount of Ag deposition was small in P-ECD (Fig. 2), the signal of Ag would be lower than that of B-ECD. For the N 1s signal, although an apparent peak was confirmed in the P-ECD, this signal was not obtained in the B-ECD (Fig. S5(c), ESI†). PVP is composed of C, O, and N atoms, whereas PVB is composed of only C and O atoms. Therefore, the presence of the N 1s XPS signal indicated the existence of PVP molecules on the AgNPs, demonstrating that it acted as a capping agent.

The capping effect of the PVP present in the deposited AgNPs on the retention time of cyan coloration in the EC device was evaluated. Because the deposited AgNPs were dissolved by Cu^{2+} ions in the EC electrolyte, the color retention properties of the EC device were insufficient. In our previous study, instead

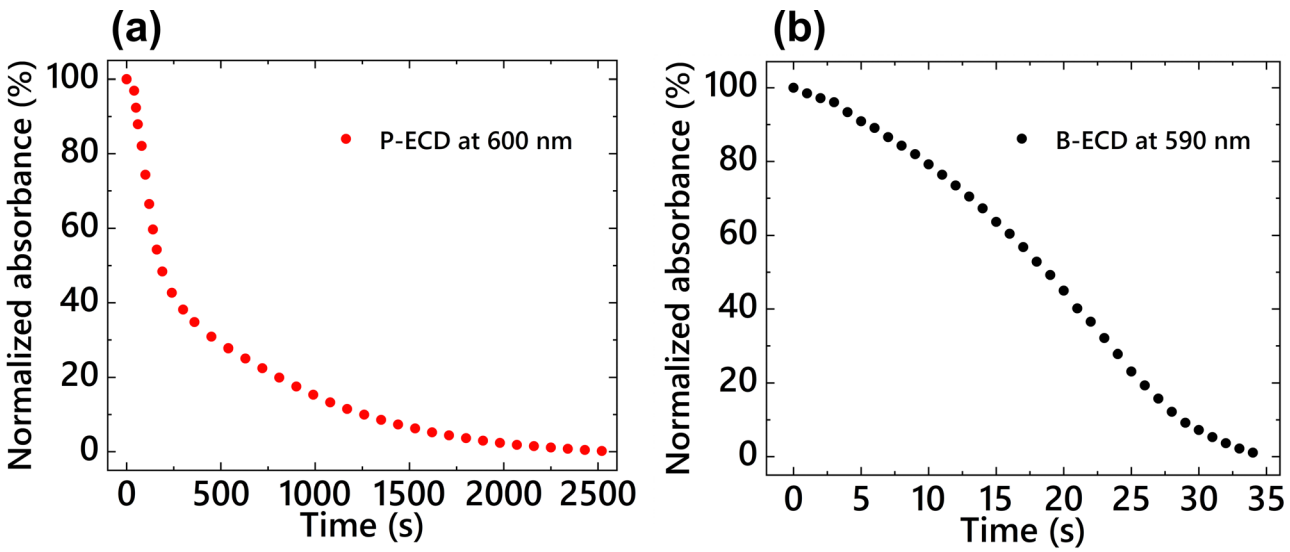

Fig. 7 Change in absorbance at the peak wavelength in Fig. 5 (at 600 nm for P-ECD and at 590 nm for B-ECD) after applying cyan coloration voltage ((a) P-ECD: V = −2.5 V, t = 120 s and (b) B-ECD: V_1 = −3.5 V, t_1 = 100 ms, V_2 = −1.6 V, t_2 = 60 s). The absorbance at each wavelength was normalized to 100% at the end of the voltage application.

of Cu^{2+} ions, the immobilization of charge compensation materials on the counter electrode was expected to improve color retention.[45,73] The monitored wavelength was the peak wavelength of the absorption band shown in Fig. 5 (600 nm for P-ECD and 590 nm for B-ECD). The absorbance at the end of the voltage application was normalized to 100%, and the transient change in the absorbance under open-circuit conditions is shown in Fig. 7. Compared to B-ECD, P-ECD exhibited obvious long color retention properties. For the P-ECD (Fig. 7(a)), the absorbance at 600 nm immediately decreased to 50% but the subsequent decrease was gradual, resulting in a retention time (defined as the time when the absorbance decreased to 10% of the initial absorbance) of 1258 s. On the other hand, the absorbance of the B-ECD (Fig. 7(b)) at 590 nm decreased immediately under the open-circuit conditions, and the retention time was 29 s. Incidentally, the viscosities of PVP- and PVB-based electrolytes were 960 mPa s and 750 mPa s, respectively. Although the diffusion coefficient is generally inversely proportional to the viscosity of a liquid, the results of retention time greatly exceeded the difference in viscosity. Therefore, the improvement in the retention time of cyan coloration could be attributed to the capping of the AgNPs by the PVP molecules. The capping effect of PVP prevented Cu^{2+} ions from approaching the electrodeposited AgNPs, and the dissolution of AgNPs was suppressed significantly. Thus, the color retention characteristics of the EC device were improved by the addition of only PVP. As previously mentioned, the P-ECD returned to a transparent state by applying a higher dissolution voltage than that of the B-ECD, although PVP suppressed the Cu ions working as an electrochemical mediator.

Since the nucleation reaction occurs continuously during the application of a constant voltage, precise control of the density of electrodeposited AgNPs is difficult. Thus, only cyan coloration was achieved by the application of a constant voltage to the P-ECD. To represent other chromatic colors from the P-ECD, the LSPR bands were tuned by controlling the morphology of the deposited AgNPs. In this study, we attempted to manipulate the interparticle coupling state by dissolving a portion of the deposited AgNPs. By dissolving the AgNPs, the LSPR absorption band due to plasmon coupling can be controlled, resulting in chromatic colors other than cyan. An Ag deposition voltage of $V = -2.6$ V was first applied to the P-ECD for 60 s, followed by a subsequent Ag dissolution voltage of V_d = 0 V (short-circuit condition) for 30 s (t_d). The absorption spectra at t = 60 and t_d = 30 s (after the application of the Ag deposition and dissolution voltages, respectively) are shown in Fig. 8(a). The absorption spectrum at t = 60 s exhibited two distinct LSPR peaks at 480 and 570 nm. The absorption band at approximately 480 nm was attributed to the LSPR of a single AgNP and the band at 570 nm was attributed to the LSPR of plasmon coupling. Upon application of the dissolution voltage, the absorption band at 570 nm disappeared, and a vivid yellow coloration was observed in the P-ECD with absorption bands below 480 nm (Fig. 8(b)). The decrease in particle size by electrochemical dissolution reduced the plasmon coupling between the AgNPs, resulting in a yellow coloration owing to the LSPR absorption of isolated AgNPs at shorter wavelengths of approximately 400–480 nm.

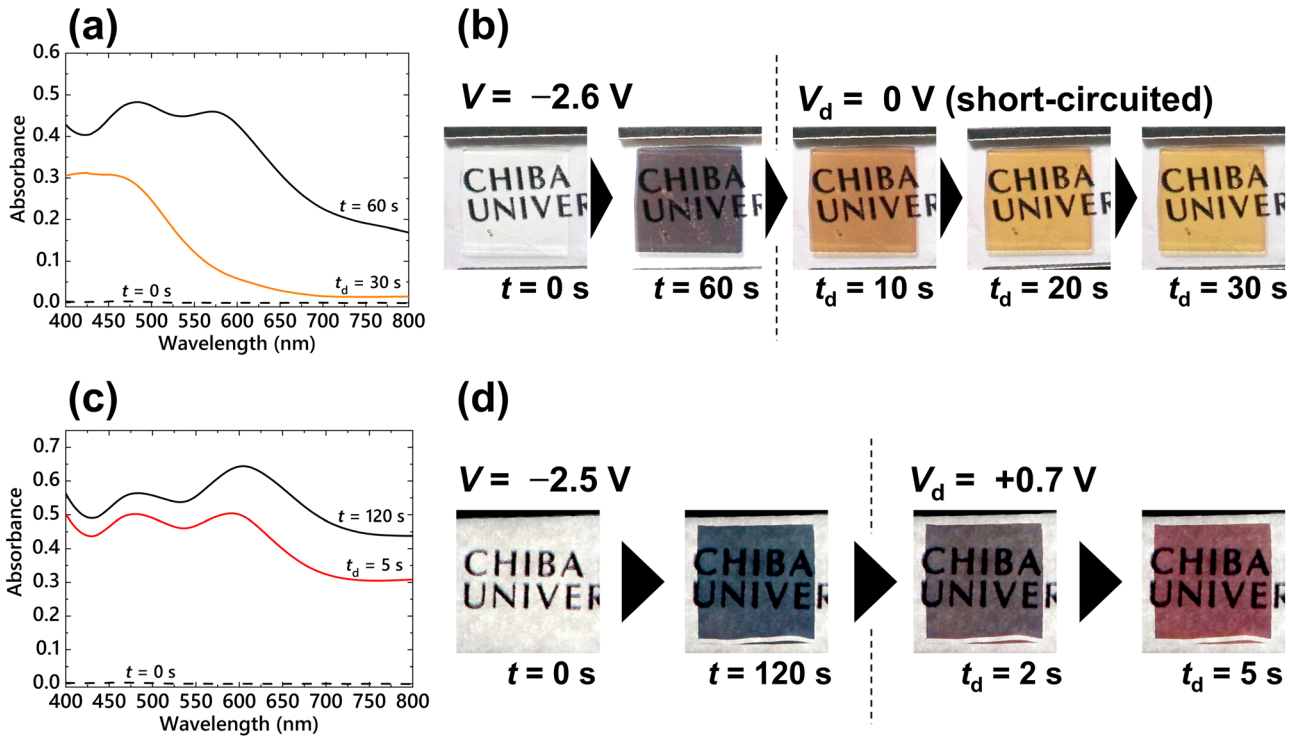

Fig. 8 The absorption spectra (a) and device images (b) of P-ECD during voltage application (V = −2.6 V, t = 60 s, V_d = 0 V, t_d = 30 s). The absorption spectra (c) and device images (d) of P-ECD during voltage application (V = −2.5 V, t = 120 s, V_d = +0.7 V, t_d = 5 s).

A $V = -2.5$ V voltage was applied to the P-ECD for 120 s in order to deposit AgNPs, and a subsequent $V_d = +0.7$ V voltage was continuously applied for 5 s (t_d) to partially dissolve the AgNPs. The absorption spectra obtained after applying the deposition (t = 120 s) and dissolution (t_d = 5 s) voltages are shown in Fig. 8(c). After applying the Ag deposition voltage, LSPR absorption peaks appeared at 480 and 610 nm. Subsequently, the LSPR absorbance at longer wavelengths (650 nm) decreased due to the application of the dissolution voltage, resulting in the appearance of red coloration (Fig. 8(d)). Since the dissolution of the AgNPs weakened the interaction of the plasmon couplings, the LSPR absorption band ascribed to the coupling (650 nm) decreased. In both absorption spectra of Fig. 8(a and c), the absorbance based on the LSPR of the single AgNPs around 480 nm was maintained in comparison with the absorbance due to plasmon coupling at 570 or 610 nm. This means that the morphological changes of single AgNPs during the dissolution process were very small. Plasmon coupling is a very delicate interaction and is greatly affected by slight changes in the relative position and size of the plasmonic particles.[43] Hence, the change of the size of the AgNPs on the order of a few nanometers significantly influenced plasmon coupling, resulting in a drastic color change of the EC device. Because Cu^{2+} ions immediately dissolve the deposited AgNPs, it has been difficult to control the coloration using such a dissolution process in previously reported PVB-based EC devices. Control of plasmon coupling by the dissolution process was facilitated by the adsorption of PVP on the surface of the AgNPs, which prevented Cu^{2+} ion contact (Fig. 7). Thus, a stable multicolor representation in P-ECD was successfully achieved using the dissolution process without the previous voltage-step method, which required precise voltage control in a few tens of milliseconds.

4. Conclusions

PVP was introduced as a capping agent to prevent aggregation of AgNPs in an Ag deposition-based EC device. PVP was expected to act as a capping agent for AgNPs, even in an electrochemical system similar to chemical reaction-based synthesis. In this study, the effects of introducing PVP on the electrochemical, morphological, and optical properties of an EC device were evaluated.

As a result, through the coordination of the PVP molecules with Ag^+ ions in the EC electrolyte, the reduction potential was positively shifted from -1.28 to -1.15 V (*vs.* Ag/Ag^+). Furthermore, PVP possibly affected the generation of Cu^+ ions in the EC electrolysis solution, resulting in a significant reduction in the operating voltage of the two-electrode EC device. Owing to the suppression of the aggregation and growth of the AgNPs in the P-ECD, as compared to the B-ECD, a vivid cyan color was obtained by applying a constant voltage in the coloration process. The morphological control of the deposited AgNPs indicated that PVP acted as a capping agent for the AgNPs, even during the electrochemical deposition process. Additionally, the color retention time of the P-ECD was significantly improved compared to that of the B-ECD. This could be attributed to the capping effect of PVP, which prevented Cu^{2+} ions from approaching the deposited AgNPs. By utilizing this improved color retention time, the LSPR bands could be manipulated by dissolving part of the deposited AgNPs to obtain other chromatic colors. As a result, vivid yellow and red colors were obtained without the previous voltage-step method, which required precise voltage control.

In this study, a novel method for controlling the shapes and sizes of electrodeposited AgNPs was demonstrated by the introduction of a capping agent into an Ag deposition-based EC device. The precise control of the morphology of electrochemically generated metal nanoparticles is expected to contribute to a wide range of fields, such as precious metal catalysts and biosensors using plasmonic particles, in addition to Ag LSPR-based electrochromism.

Conflicts of interest

There are no conflicts to declare.

Acknowledgements

This study was supported by JSPS KAKENHI (15H03880, 17H06377, 19J21962, and 22H02154), JST (A-STEP: AS2915036S), the establishment of university fellowships for the creation of science technology innovation (JPMJFS2107), and Sasakawa Scientific Research Grant (2023-2022).

References

1 A. A. Argun, P. H. Aubert, B. C. Thompson, I. Schwendeman, C. L. Gaupp, J. Hwang, N. J. Pinto, D. B. Tanner, A. G. MacDiarmid and J. R. Reynolds, *Chem. Mater.*, 2004, **16**, 4401–4412.
2 A. Watanabe, K. Mori, Y. Iwasaki, Y. Nakamura and S. Niizuma, Electrochromism of Polyaniline Film Prepared by Electrochemical Polymerization, *Macromolecules*, 1987, **20**, 1793–1796.
3 M. Higuchi and Y. Fujii, Designed, Flexible Electrochromic Display Device with Fe(II)-Based Metallo-Supramolecular Polymer Using Mechanically Etched ITO Film, *J. Photopolym. Sci. Technol.*, 2021, **34**, 175–180.
4 I. Mjejri, C. M. Doherty, M. Rubio-Martinez, G. L. Drisko and A. Rougier, Double-Sided Electrochromic Device Based on Metal-Organic Frameworks, *ACS Appl. Mater. Interfaces*, 2017, **9**, 39930–39934.
5 H. Urano, S. Sunohara, H. Ohtomo and N. Kobayashi, Electrochemical and spectroscopic characteristics of dimethyl terephthalate, *J. Mater. Chem.*, 2004, **14**, 2366–2368.
6 A. S. Ribeiro, V. C. Nogueira, P. Faria dos Santos Filho and M. A. De Paoli, Electrochromic properties of poly{3-[12-(p-methoxyphenoxy)dodecyl]thiophene}, *Electrochim. Acta*, 2004, **49**, 2237–2242.

7 S. H. Hsiao and Y. Z. Chen, Electrosynthesis of redox-active and electrochromic polymer films from triphenylamine-cored star-shaped molecules end-capped with arylamine groups, *Eur. Polym. J.*, 2018, **99**, 422–436.
8 Z. Liang, K. Nakamura and N. Kobayashi, A multicolor electrochromic device having hybrid capacitor architecture with a porous carbon electrode, *Sol. Energy Mater. Sol. Cells*, 2019, **200**, 109914.
9 R. J. Mortimer, Organic electrochromic materials, *Electrochim. Acta*, 1999, **44**, 2971–2981.
10 P. H. L. Noltent, M. Kremers and R. Griessen, Optical Switching of Y-Hydride Thin Film Electrodes, *J. Electrochem. Soc.*, 1996, **143**, 455.
11 T. J. Richardson, J. L. Slack, B. Farangis and M. D. Rubin, Mixed metal films with switchable optical properties, *Appl. Phys. Lett.*, 2002, **80**, 1349–1351.
12 K. Tajima, Y. Yamada, M. Okada and K. Yoshimura, Surface coating of electrochromic switchable mirror glass based on Mg-Ni thin film for high durability in the environment, *Appl. Phys. Express*, 2010, **3**, 042201.
13 Y. Kondo, H. Tanabe, H. Kudo, K. Nakano and T. Otake, Electrochromic Type E-Paper Using Poly(1H-Thieno[3,4-d] Imidazol-2(3H)-One) Derivatives by a Novel Printing Fabrication Process, *Materials*, 2011, **4**, 2171–2182.
14 N. Kobayashi, S. Miura, M. Nishimura and H. Urano, Organic electrochromism for a new color electronic paper, *Sol. Energy Mater. Sol. Cells*, 2008, **92**, 136–139.
15 D. Corr, U. Bach, D. Fay, M. Kinsella, C. McAtamney, F. O'Reilly, S. N. Rao and N. Stobie, Coloured electrochromic 'paper-quality' displays based on modified mesoporous electrodes, *Solid State Ionics*, 2003, **165**, 315–321.
16 C. G. Granqvist, Electrochromic tungsten oxide ''lms: Review of progress 1993-1998, *Sol. Energy Mater. Sol. Cells*, 2000, **60**, 201–262.
17 D. R. Rosseinsky and R. J. Mortimer, Electrochromic Systems and the Prospects for Devices**, *Adv. Mater.*, 2001, **13**, 783–793.
18 U. Bach, D. Corr, D. Lupo, F. Pichot and M. Ryan, Nanomaterials-Based Electrochromics for Paper-Quality Displays**, *Adv. Mater.*, 2002, **14**, 845–848.
19 D. T. Gillaspie, R. C. Tenent and A. C. Dillon, Metal-oxide films for electrochromic applications: Present technology and future directions, *J. Mater. Chem.*, 2010, **20**, 9585–9592.
20 G. A. Niklasson and C. G. Granqvist, Electrochromics for smart windows: Thin films of tungsten oxide and nickel oxide, and devices based on these, *J. Mater. Chem.*, 2007, **17**, 127–156.
21 C. G. Granqvist, *Thin Solid Films*, 2014, **564**, 1–38.
22 T. J. Richardson, J. L. Slack, R. D. Armitage, R. Kostecki, B. Farangis and M. D. Rubin, Switchable mirrors based on nickel-magnesium films, *Appl. Phys. Lett.*, 2001, **78**, 3047–3049.
23 S. H. Lee, R. Deshpande, P. A. Parilla, K. M. Jones, B. To, A. H. Mahan and A. C. Dillon, Crystalline WO_3 nanoparticles for highly improved electrochromic applications, *Adv. Mater.*, 2006, **18**, 763–766.
24 K. R. Reyes-Gil, Z. D. Stephens, V. Stavila and D. B. Robinson, Composite WO_3/TiO_2 nanostructures for high electrochromic activity, *ACS Appl. Mater. Interfaces*, 2015, **7**, 2202–2213.
25 S. H. Baeck, K. S. Choi, T. F. Jaramillo, G. D. Stucky and E. W. McFarland, Enhancement of photocatalytic and electrochromic properties of electrochemically fabricated mesoporous WO_3 thin films, *Adv. Mater.*, 2003, **15**, 1269–1273.
26 X. H. Xia, J. P. Tu, J. Zhang, X. L. Wang, W. K. Zhang and H. Huang, Electrochromic properties of porous NiO thin films prepared by a chemical bath deposition, *Sol. Energy Mater. Sol. Cells*, 2008, **92**, 628–633.
27 K. H. Kim, M. Kahuku, Y. Abe, M. Kawamura and T. Kiba, Improved electrochromic performance in nickel oxide thin film by Zn doping, *Int. J. Electrochem. Sci.*, 2020, **15**, 4065–4071.
28 D. Dixit and K. V. Madhuri, Electrochromism in MoO_3 nanostructured thin films, *Superlattices Microstruct.*, 2021, **156**, 106936.
29 C. Park, S. Seo, H. Shin, B. D. Sarwade, J. Na and E. Kim, Switchable silver mirrors with long memory effects, *Chem. Sci.*, 2015, **6**, 596–602.
30 X. Hou, Z. Wang, Z. Zheng, J. Guo, Z. Sun and F. Yan, Poly(ionic liquid) Electrolytes for a Switchable Silver Mirror, *ACS Appl. Mater. Interfaces*, 2019, **11**, 20417–20424.
31 S. M. Cho, S. Kim, T. Y. Kim, C. S. Ah, J. Song, S. H. Cheon, J. Y. Kim, H. Ryu, Y. H. Kim, C. S. Hwang and J. I. Lee, New switchable mirror device with a counter electrode based on reversible electrodeposition, *Sol. Energy Mater. Sol. Cells*, 2018, **179**, 161–168.
32 K. R. Jeong, I. Lee, J. Y. Park, C. S. Choi, S. H. Cho and J. L. Lee, Enhanced black state induced by spatial silver nanoparticles in an electrochromic device, *NPG Asia Mater.*, 2017, **9**, e362.
33 S. Araki, K. Nakamura, K. Kobayashi, A. Tsuboi and N. Kobayashi, Electrochemical optical-modulation device with reversible transformation between transparent, mirror, and black, *Adv. Mater.*, 2012, **24**, OP122–OP126.
34 A. Imamura, M. Kimura, T. Kon, S. Sunohara and N. Kobayashi, Bi-based electrochromic cell with mediator for white/black imaging, *Sol. Energy Mater. Sol. Cells*, 2009, **93**, 2079–2082.
35 S. I. Chrdoba De Torresi and I. A. Carlos, Optical characterization of bismuth reversible electrodeposition, *J. Electroanal. Chem.*, 1996, **414**, 11–16.
36 A. L. S. Eh, M. F. Lin, M. Cui, G. Cai and P. S. Lee, A copper-based reversible electrochemical mirror device with switchability between transparent, blue, and mirror states, *J. Mater. Chem. C*, 2017, **5**, 6547–6554.
37 X. Guo, J. Chen, A. L. S. Eh, W. C. Poh, F. Jiang, F. Jiang, J. Chen and P. S. Lee, Heat-Insulating Black Electrochromic Device Enabled by Reversible Nickel-Copper Electrodeposition, *ACS Appl. Mater. Interfaces*, 2022, **14**, 20237–20246.
38 A. Tsuboi, K. Nakamura and N. Kobayashi, Multicolor electrochromism showing three primary color states (cyan-magenta-yellow) based on size- and shape-controlled silver nanoparticles, *Chem. Mater.*, 2014, **26**, 6477–6485.

39 A. Tsuboi, K. Nakamura and N. Kobayashi, Chromatic control of multicolor electrochromic device with localized surface plasmon resonance of silver nanoparticles by voltage-step method, *Sol. Energy Mater. Sol. Cells*, 2016, **145**, 16–25.
40 A. Tsuboi, K. Nakamura and N. Kobayashi, A Localized Surface Plasmon Resonance-Based Multicolor Electrochromic Device with Electrochemically Size-Controlled Silver Nanoparticles, *Adv. Mater.*, 2013, **25**, 3197–3201.
41 A. Tsuboi, K. Nakamura and N. Kobayashi, *J. Soc. Inf. Disp.*, 2013, **21**, 361–367.
42 R. Onodera, A. Tsuboi, K. Nakamura and N. Kobayashi, Coloration mechanisms of Ag deposition-based multicolor electrochromic device investigated by morphology of Ag deposit and its optical properties, *J. Soc. Inf. Disp.*, 2016, **24**, 424–432.
43 S. Kimura, T. Sugita, K. Nakamura and N. Kobayashi, An improvement in the coloration properties of Ag deposition-based plasmonic EC devices by precise control of shape and density of deposited Ag nanoparticles, *Nanoscale*, 2020, **12**, 23975–23983.
44 S. Uji, S. Kimura, K. Nakamura and N. Kobayashi, Analysis for coloration mechanism of reversible silver deposition-based electrochromic device by in situ observation of plasmonic nanoparticles with dark-field microscopy, *Sol. Energy Mater. Sol. Cells*, 2023, **251**, 112119.
45 S. Kimura, H. Wakatsuki, K. Nakamura and N. Kobayashi, Compensative Electrochromic Device Utilizing Electrodeposited Plasmonic Silver Nanoparticles and Manganese Oxide to Achieve Retention of Chromatic Color, *Electrochemistry*, 2022, **90**, 1–6.
46 D. D. Evanoff and G. Chumanov, Size-controlled synthesis of nanoparticles. 1. 'silver-only' aqueous suspensions via hydrogen reduction, *J. Phys. Chem. B*, 2004, **108**, 13948–13956.
47 T. Huang and X. H. N. Xu, Synthesis and characterization of tunable rainbow colored colloidal silver nanoparticles using single-nanoparticle plasmonic microscopy and spectroscopy, *J. Mater. Chem.*, 2010, **20**, 9867–9876.
48 E. Kazuma, T. Yamaguchi, N. Sakai and T. Tatsuma, Growth behaviour and plasmon resonance properties of photocatalytically deposited Cu nanoparticles, *Nanoscale*, 2011, **3**, 3641–3645.
49 W. Plieth, H. Dietz, A. Anders, G. Sandmann, A. Meixner, M. Weber and H. Kneppe, Electrochemical preparation of silver and gold nanoparticles: Characterization by confocal and surface enhanced Raman microscopy, *Surf. Sci.*, 2005, **597**, 119–126.
50 G. Sandmann, H. Dietz and W. Plieth, Preparation of silver nanoparticles on ITO surfaces by a double-pulse method, *J. Electroanal. Chem.*, 2000, **491**, 78–86.
51 M. Ueda, H. Dietz, A. Anders, H. Kneppe, A. Meixner and W. Plieth, Double-pulse technique as an electrochemical tool for controlling the preparation of metallic nanoparticles, *Electrochim. Acta*, 2002, **48**, 377–386.
52 Q. Wu, P. Diao, J. Sun, T. Jin, D. Xu and M. Xiang, Electrodeposition of Vertically Aligned Silver Nanoplate Arrays on Indium Tin Oxide Substrates, *J. Phys. Chem. C*, 2015, **119**, 20709–20720.
53 C. M. Cobley, S. E. Skrabalak, D. J. Campbell and Y. Xia, Shape-controlled synthesis of silver nanoparticles for plasmonic and sensing applications, *Plasmonics*, 2009, **4**, 171–179.
54 W. Jin, G. Liang, Y. Zhong, Y. Yuan, Z. Jian, Z. Wu and W. Zhang, The Influence of CTAB-Capped Seeds and Their Aging Time on the Morphologies of Silver Nanoparticles, *Nanoscale Res. Lett.*, 2019, **14**, 1–11.
55 H. S. Al-Ghamdi and W. E. Mahmoud, One pot synthesis of multi-plasmonic shapes of silver nanoparticles, *Mater. Lett.*, 2013, **105**, 62–64.
56 H. Hegde, C. Santhosh and R. K. Sinha, Seed mediated synthesis of highly stable CTAB capped triangular silver nanoplates for LSPR sensing, *Mater. Res. Express*, 2019, **6**, 105075.
57 S. Mukherji, S. Bharti, G. Shukla and S. Mukherji, Synthesis and characterization of size- And shape-controlled silver nanoparticles, *Phys. Sci. Rev.*, 2019, **4**, 20170082.
58 F. M. Balci, S. Sarisozen, N. Polat, C. M. Guvenc, U. Karadeniz, A. Tertemiz and S. Balci, Laser assisted synthesis of anisotropic metal nanocrystals and strong light-matter coupling in decahedral bimetallic nanocrystals, *Nanoscale Adv.*, 2021, **3**, 1674–1681.
59 A. A. Unal, A. Stalmashonak, H. Graener and G. Seifert, Tuning the shape anisotropy of silver nanoparticles using time-delayed laser pulse pair irradiations, *Appl. Phys. B*, 2010, **101**, 841–847.
60 K. G. Stamplecoskie and J. C. Scaiano, Light emitting diode irradiation can control the morphology and optical properties of silver nanoparticles, *J. Am. Chem. Soc.*, 2010, **132**, 1825–1827.
61 G. P. Lee, Y. Shi, E. Lavoie, T. Daeneke, P. Reineck, U. B. Cappel, D. M. Huang and U. Bach, Light-driven transformation processes of anisotropic silver nanoparticles, *ACS Nano*, 2013, **7**, 5911–5921.
62 J. H. Byeon and Y. W. Kim, A novel polyol method to synthesize colloidal silver nanoparticles by ultrasonic irradiation, *Ultrason. Sonochem.*, 2012, **19**, 209–215.
63 D. V. Radziuk, W. Zhang, D. Shchukin and H. Möhwald, Ultrasonic alloying of preformed gold and silver nanoparticles, *Small*, 2010, **6**, 545–553.
64 P. S. Mdluli, N. M. Sosibo, P. N. Mashazi, T. Nyokong, R. T. Tshikhudo, A. Skepu and E. Van Der Lingen, Selective adsorption of PVP on the surface of silver nanoparticles: A molecular dynamics study, *J. Mol. Struct.*, 2011, **1004**, 131–137.
65 M. S. Ribeiro, K. C. Ribeiro, V. M. Lenart, R. F. Turchiello and S. L. Gómez, PVP-Capped Gold Nanoparticles: Thermal Nonlinear Refraction Probed by Spatial Self-Phase Modulation, *Phys. Status Solidi A*, 2022, **219**, 2100600.
66 A. Sarkar, T. Mukherjee and S. Kapoor, PVP-stabilized copper nanoparticles: A reusable catalyst for 'click' reaction between terminal alkynes and azides in nonaqueous solvents, *J. Phys. Chem. C*, 2008, **112**, 3334–3340.

67 R. Kimura, A. Tsuboi, K. Nakamura and N. Kobayashi, Effects of silver halide complexes on optical and electrochemical properties of silver deposition-based electrochromic device, *Sol. Energy Mater. Sol. Cells*, 2018, **177**, 128–133.
68 Z. Zhang, B. Zhao and L. Hu, PVP Protective Mechanism of Ultrafine Silver Powder Synthesized by Chemical Reduction Processes, *J. Solid State Chem.*, 1996, **121**, 105–110.
69 K. V. Anasuya, M. K. Veeraiah and P. Hemalatha, Synthesis and Characterisation of Poly(Vinylpyrrolidone)–Copper(II) Complexes, Research, *J. Chem. Sci.*, 2015, **5**, 64–69.
70 S. Tsuneyasu, Y. Watanabe, K. Nakamura and N. Kobayashi, *In situ* measurements of electrode potentials of anode and cathode in organic electrochromic devices, *Sol. Energy Mater. Sol. Cells*, 2017, **163**, 200–203.
71 Q. Wei, E. McLeod, H. Qi, Z. Wan, R. Sun and A. Ozcan, On-chip cytometry using plasmonic nanoparticle enhanced lensfree holography, *Sci. Rep.*, 2013, **3**, 1699.
72 C. Sönnichsen, B. M. Reinhard, J. Liphardt and A. P. Alivisatos, A molecular ruler based on plasmon coupling of single gold and silver nanoparticles, *Nat. Biotechnol.*, 2005, **23**, 741–745.
73 S. Kimura, K. Nakamura and N. Kobayashi, Bistable silver electrodeposition-based EC device with a Prussian blue counter electrode to maintain the mirror state without power supply, *Sol. Energy Mater. Sol. Cells*, 2020, **205**, 110247.

